Available online at www.sciencedirect.com
SCIENCE DIRECT®
Ocean Modelling 12 (2006) 205–223
Ocean Modelling
www.elsevier.com/locate/ocemod

An adaptive finite element water column model using the Mellor–Yamada level 2.5 turbulence closure scheme

Emmanuel Hanert [a,b,*], Eric Deleersnijder [a,b], Vincent Legat [b]

[a] *Institut d'Astronomie et de Géophysique G. Lemaître, Université catholique de Louvain, 2 Chemin du cyclotron, B-1348 Louvain-la-Neuve, Belgium*
[b] *Centre for Systems Engineering and Applied Mechanics, Université catholique de Louvain, 4 Avenue Georges Lemaître, B-1348 Louvain-la-Neuve, Belgium*

Received 31 January 2005; received in revised form 20 May 2005; accepted 20 May 2005
Available online 29 June 2005

Abstract

A one-dimensional water column model using the Mellor and Yamada level 2.5 parameterization of vertical turbulent fluxes is presented. The model equations are discretized with a mixed finite element scheme. Details of the finite element discrete equations are given and adaptive mesh refinement strategies are presented. The refinement criterion is an "a posteriori" error estimator based on stratification, shear and distance to surface. The model performances are assessed by studying the stress driven penetration of a turbulent layer into a stratified fluid. This example illustrates the ability of the presented model to follow some internal structures of the flow and paves the way for truly generalized vertical coordinates.

Keywords: Mellor and Yamada; Turbulence closure; Finite elements; Adaptivity; Mixed layer deepening

* Corresponding author. Address: Institut d'Astronomie et de Géophysique G. Lemaître, Université catholique de Louvain, 2 Chemin du cyclotron, B-1348 Louvain-la-Neuve, Belgium.
E-mail address: hanert@astr.ucl.ac.be (E. Hanert).

1463-5003/$ - see front matter
doi:10.1016/j.ocemod.2005.05.003

1. Introduction

In many marine modelling applications, a reliable parameterization of eddy coefficients is needed to accurately represent vertical turbulent fluxes. Nowadays, most ocean models use one- or two-equation turbulence closures. The most popular are the Mellor and Yamada (1982) level 2.5 model and the k–ε model (e.g., Rodi, 1987). A detailed comparison of both models has been performed by Burchard et al. (1998) and Burchard and Petersen (1999). Beside these two models, other two-equation models exist, like the k–ω model, introduced by Wilcox (1988) and extended to buoyancy affected flows by Umlauf et al. (2003). Although all three models have very similar physical parameterizations (Umlauf and Burchard, 2003), only the model of Mellor and Yamada took stratification into account since its inception. As a result, it has been used frequently in atmospheric and oceanic applications (e.g., Yamada, 1983; Blumberg and Mellor, 1987; Rosati and Miyakoda, 1988; Timmermann and Beckmann, 2004).

The numerical discretization of such turbulence closures is usually accomplished in finite differences, on a staggered or non-staggered grid. Details of the discretization of the turbulence energy equations, on different finite difference grids and with various time discretization have been given in Davies and Jones (1991) and Burchard (2002a). For problems in which the shape of eddy viscosity is constant in time, although its magnitude may change, functional approaches have been suggested (Davies, 1987). More recently, Burchard (2002b) proposed an energy-conserving discretization of the shear and production terms for the turbulent kinetic energy. The issue of non-uniform adaptive vertical grids has been studied by Burchard and Beckers (2004). They proposed a finite difference scheme using a grid that can follow the relevant internal structures of the flow.

Common to all the previous works is the use of the finite difference method to discretize the hydrodynamic equations. However, over recent years other numerical methods have been contemplated for simulating oceanic and coastal flows. These are mainly the finite element (e.g., Lynch et al., 1996; Le Roux et al., 2000; Danilov et al., 2004; Ford et al., 2004a,b; Hanert et al., 2005), the finite volume (e.g., Casulli and Walters, 2000; Chen et al., 2003) and the spectral element (e.g., Iskandarani et al., 1995, 2003) methods. Their principal advantage is that they allow the use of unstructured meshes. Such meshes have proved to be particularly well suited to represent localized phenomena and complex geometries (Legrand et al., 2000). They also provide a natural framework to perform dynamical mesh adaptation (Piggot et al., 2005). This seems to be a very promising tool for use in 3D ocean modelling as it permits to adapt the mesh in both space and time. Therefore, an optimal use of the computational power is always possible as the mesh "follows" the dynamically active regions. Until now, most of the work on unstructured mesh ocean modelling has focused on horizontal processes while little interest has been paid to the discretization of vertical ones.

The purpose of this paper is to investigate the ability of the finite element method, combined with adaptive mesh procedures, to discretize vertical oceanic processes. As a test problem, we simulate the stress-driven deepening of the ocean mixed layer by using Mellor–Yamada level 2.5 turbulence closure scheme. This phenomenon exhibits a transient dynamics and is therefore well suited to assess mesh adaptivity methods. All simulations have been performed with a MATLAB software, which is freely available at the following address: http://www.mema.ucl.ac.be/~hanert/FEMY25.html. This is a way to provide all numerical and technical tricks required to obtain an accurate solution of this non-linear problem. While the MATLAB programming language is well

suited for educational purposes, it is not the most efficient for heavy computations. In that respect, the finite difference General Ocean Turbulence Model (GOTM, http://www.gotm.net) provides a comprehensive package of efficient turbulence models.

2. A simple water column model

For some very idealized situations where all variables are horizontally homogeneous, the following one-dimensional water column model may be used:

$$\frac{\partial \mathbf{u}}{\partial t} + f\,\mathbf{e}_z \times \mathbf{u} = \frac{\partial}{\partial z}\left(K_u \frac{\partial \mathbf{u}}{\partial z}\right), \tag{1}$$

$$\frac{\partial b}{\partial t} = \frac{\partial}{\partial z}\left(K_b \frac{\partial b}{\partial z}\right), \tag{2}$$

where f is the Coriolis factor, z is the vertical coordinate (increasing upward), $\mathbf{e}_z$ is the vertical unit vector, K_u is the eddy viscosity and K_b is the eddy diffusivity. The unknowns are the horizontal velocity $\mathbf{u} = (u, v)$ and the buoyancy $b = -g(\rho - \rho_0)/\rho_0$, where g is the gravitational acceleration, ρ is the water density and ρ_0 is a reference value of the density. The model domain is a water column that goes from $z = -h$ to the sea surface ($z = 0$). The initial and boundary conditions depend on the problem under consideration and will be specified later.

In Eqs. (1) and (2), eddy coefficients are parameterized with the Mellor–Yamada level 2.5 turbulence closure:

$$K_u = lqS_u,$$

$$K_b = lqS_b,$$

where l and q are, respectively, an appropriate length scale, termed the turbulence macroscale, and a velocity scale, obtained from the turbulent kinetic energy $k = q^2/2$. The stability functions S_u and S_b are dimensionless functions of G_M and G_H:

$$(G_M, G_H) = \frac{l^2}{q^2}(M^2, -N^2),$$

where M and N are the Prandtl and Brunt-Väisälä frequencies, i.e.,

$$(M^2, N^2) = \left(\left\|\frac{\partial \mathbf{u}}{\partial z}\right\|^2, \frac{\partial b}{\partial z}\right).$$

The usual Eulerian norm is denoted $\|\cdot\|$.

The velocity and length scales obey the following equations:

$$\frac{\partial q^2}{\partial t} = 2K_u M^2 - 2K_b N^2 - \frac{2q^3}{16.6l} + \frac{\partial}{\partial z}\left(K_q \frac{\partial q^2}{\partial z}\right), \tag{3}$$

$$\frac{\partial q^2 l}{\partial t} = 1.8lK_u M^2 - 1.8lK_b N^2 - \frac{Wq^3}{16.6} + \frac{\partial}{\partial z}\left(K_q \frac{\partial q^2 l}{\partial z}\right). \tag{4}$$

The eddy diffusivity of the turbulence model equations is $K_q = 0.2lq$. The physical meaning of the various terms in Eq. (3) is the following: $K_u M^2$ is the shear production of turbulent kinetic energy

(TKE), $K_b N^2$ is the TKE conversion into potential energy and $q^3/(16.6l)$ represents the viscous dissipation of TKE.

To compute K_u and K_b, we use the stability functions designed by Galperin et al. (1988):

$$S_u = \frac{0.393 - 3.085 G_H}{1 - 40.803 G_H + 212.469 G_H^2},$$

$$S_b = \frac{0.494}{1 - 34.676 G_H}.$$

In addition, the following constraints are necessary:

$$l^2 \leqslant \frac{0.28 q^2}{\max(0, N^2)}, \quad -0.28 \leqslant G_H \leqslant 0.0233. \tag{5}$$

All the empirical parameters used in the turbulence closure model are motivated by Mellor and Yamada (1974, 1982) and Galperin et al. (1988).

In addition, the Mellor–Yamada model requires the introduction of a wall proximity function, W, to be able to represent the logarithmic layer near boundaries. In the standard implementation of the model, this function is defined as

$$W = 1 + \frac{1.33 l^2}{(\kappa L)^2},$$

where $\kappa \simeq 0.4$ is the von Karman constant and L is a function of the distance to the seabed, d_b, and of the distance to the sea surface, d_s: $L = d_s d_b/(d_s + d_b)$. It should be noted that when the distance to the sea bottom is assumed infinite, $L = d_s = |z|$. In that case, the wall proximity function may be written as $W = 1 + \frac{1.33 l^2}{(\kappa z)^2}$. Other wall proximity functions have also been suggested (Burchard et al., 1998; Blumberg et al., 1992).

Beside the necessity to use a wall proximity function, another shortcoming of the Mellor–Yamada model is that the empirical coefficients for the buoyancy and for the shear production terms are the same. As a result, the turbulence closure does not take into account the limiting effects of stable stratification on the size of turbulent eddies (Galperin et al., 1988). To overcome this issue, the length scale limitation (5) has been suggested. Another remedy is to properly calibrate the buoyancy production term. In that case, the model works well without the length scale limitation (Burchard, 2001). Burchard and Bolding (2001) have also reported that the maximum value of the Richardson number, $Ri = 0.2$, that can be reached with the stability functions of Galperin et al. (1988) is too small. As a result, the model does not reach high turbulent Prandtl numbers. The turbulence closure of Mellor–Yamada has been improved by several authors in recent years (e.g., Kantha and Clayson, 1994; Canuto et al., 2001).

3. Numerical scheme

3.1. Finite element spatial discretization

The derivation of the finite element discretization is based on a variational or weak formulation (Ciarlet, 1978; Johnson, 1990) of the model equations (1)–(4). If the model domain is $\Omega = [-h, 0]$, the weak formulation of Eq. (1) reads:

$$\int_{-h}^{0} \frac{\partial \mathbf{u}}{\partial t} \cdot \hat{\mathbf{u}}\,\mathrm{d}z + \int_{-h}^{0} f(\mathbf{e}_z \times \mathbf{u}) \cdot \hat{\mathbf{u}}\,\mathrm{d}z = \int_{-h}^{0} \frac{\partial}{\partial z}\left(K_u \frac{\partial \mathbf{u}}{\partial z}\right) \cdot \hat{\mathbf{u}}\,\mathrm{d}z$$
$$= -\int_{-h}^{0} K_u \frac{\partial \mathbf{u}}{\partial z} \cdot \frac{\partial \hat{\mathbf{u}}}{\partial z}\,\mathrm{d}z + \left[K_u \frac{\partial \mathbf{u}}{\partial z} \cdot \hat{\mathbf{u}}\right]_{z=-h}^{z=0}, \tag{6}$$

where $\hat{\mathbf{u}}$ is an arbitrary weighting function that belongs to the Sobolev space $H^1(\Omega)$ and $\left(\rho K_u \frac{\partial \mathbf{u}}{\partial z} \cdot \hat{\mathbf{u}}\right)_{z=z_k}$ (where $z_k = -h, 0$) can be viewed as a momentum flux at the bottom and at the surface respectively. It is readily seen that Neumann boundary conditions can be naturally enforced in the weak formulation thanks to the integration by parts. The weak formulation of Eqs. (2)–(4) is derived in the same way.

Afterwards, one has to build a discrete approximation of the exact solution $\mathbf{u}$. The discrete solution, denoted $\mathbf{u}^h$, is associated with a partition of the computational domain into N_E non-overlapping elements or intervals Ω_e ($1 \leqslant e \leqslant N_E$):

$$\bar{\Omega} = \bigcup_{e=1}^{N_E} \bar{\Omega}_e \quad \text{and} \quad \Omega_e \cap \Omega_f = \emptyset \quad \text{for } e \neq f,$$

where $\bar{\Omega}$ is the closure of Ω. The discrete solution can be expressed in terms of basis functions ϕ_i:

$$\mathbf{u}^h(t,z) = \sum_{i=1}^{N} \mathbf{u}_i(t)\phi_i(z), \tag{7}$$

where $\mathbf{u}_i$ are the unknown velocity nodal values. The number of velocity degrees of freedom is denoted N. Basis functions are low order polynomials (constant, linear, quadratic, etc.) equal to one on a mesh node and equal to zero on all the other nodes. They are therefore referred to as piecewise polynomials. For a given mesh, one may build a number of finite element schemes simply by changing the nodes distribution on each element. Fig. 1 shows a 1D mesh where there are either 1, 2, 3 or 4 nodes per element. The corresponding basis functions are constant, linear, quadratic and cubic respectively.

The nodal values are found by applying the Galerkin procedure, which amounts to replace $\mathbf{u}$ by $\mathbf{u}^h$ and $\hat{\mathbf{u}}$ by $(\phi_i, 0)$ or $(0, \phi_i)$ ($1 \leqslant i \leqslant N$) in (6). Then, one obtains the following set of discrete equations:

$$\int_{-h}^{0} \frac{\partial u^h}{\partial t}\phi_i\,\mathrm{d}z - f\int_{-h}^{0} v^h\phi_i\,\mathrm{d}z = -\int_{-h}^{0} K_u \frac{\partial u^h}{\partial z}\frac{\partial \phi_i}{\partial z}\,\mathrm{d}z + \left[K_u \frac{\partial u^h}{\partial z}\phi_i\right]_{z=-h}^{z=0}, \tag{8}$$

$$\int_{-h}^{0} \frac{\partial v^h}{\partial t}\phi_i\,\mathrm{d}z + f\int_{-h}^{0} u^h\phi_i\,\mathrm{d}z = -\int_{-h}^{0} K_u \frac{\partial v^h}{\partial z}\frac{\partial \phi_i}{\partial z}\,\mathrm{d}z + \left[K_u \frac{\partial v^h}{\partial z}\phi_i\right]_{z=-h}^{z=0}. \tag{9}$$

It should be noted that more sophisticated techniques, like the Discontinuous Galerkin method (Johnson, 1990; Cockburn et al., 2000), could also be used to derive the discrete equations in order to improve the accuracy and the robustness of the numerical scheme. In particular, this technique is mandatory for a piecewise constant approximation. By using (7), one may rewrite Eqs. (8) and (9) in matrix form:

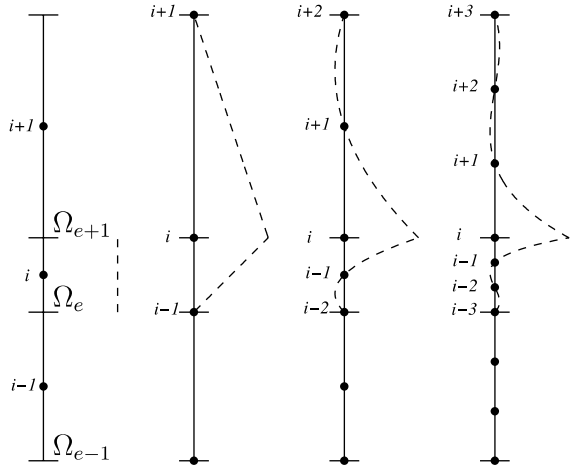

Fig. 1. Example of a 1D finite element mesh with different interpolations using, from the left to the right, constant, linear, quadratic and cubic basis functions. The model variables are computed on mesh nodes (represented by "●"). For each mesh, the basis function associated with node i is represented. The three elements of the mesh are denoted Ω_{e-1}, Ω_e and Ω_{e+1}.

$$\mathsf{M}_{ij}\left(\frac{\mathrm{d}u_j}{\mathrm{d}t} - fv_j\right) = \mathsf{D}_{ij}u_j,$$
$$\mathsf{M}_{ij}\left(\frac{\mathrm{d}v_j}{\mathrm{d}t} + fu_j\right) = \mathsf{D}_{ij}v_j,$$

where $\mathsf{M}_{ij} = \int_{-h}^{0} \phi_i\phi_j \,\mathrm{d}z$ is the mass matrix and $\mathsf{D}_{ij} = -\int_{-h}^{0} K_u \frac{\partial\phi_i}{\partial z}\frac{\partial\phi_j}{\partial z}\,\mathrm{d}z$ is the stiffness matrix. These integrals are easily computed as they only involve products of low order polynomials or products of their derivatives. The derivation of the discrete formulation of Eqs. (2)–(4) is similar, although some integrals may be more difficult to compute because of the non-linear terms in the turbulent variables equations.

In 1D, it is well known that finite element discrete equations are very close to those obtained with the finite difference method. Indeed, a finite element scheme using nth order basis functions is similar to a $(n+1)$th order finite difference scheme. It is possible to obtain exactly the same discrete equations by using a Dirac delta as weighting function in formulation (6). This amounts to replace $\hat{\mathbf{u}}$ by $(\delta(x-x_i),0)$ or $(0,\delta(x-x_i))$ $(1 \leqslant i \leqslant N)$. That method is usually referred to as collocation. In 1D, the main advantage of the finite element method is that it may accommodate uniform and non-uniform grids without any modifications. The accuracy of the method may also be easily changed by increasing or decreasing the order of the basis functions.

In this work, we have used piecewise linear basis functions to approximate u, v, b, q^2 and q^2l. Therefore, the slope of the velocity and buoyancy, as well as the Prandtl and Brunt-Väisälä frequencies, are piecewise constant. The eddy coefficients are computed on the vertices and are linearly interpolated on each element. Theoretically, the numerical scheme is second-order accurate in space.

3.2. Temporal discretization

Eqs. (1)–(4) are discretized in time by using the following scheme:

$$\frac{\mathbf{u}^{n+1}-\mathbf{u}^{n}}{\Delta t}=-f\mathbf{e}_z\times\frac{\mathbf{u}^{n+1}+\mathbf{u}^{n}}{2}+\frac{\partial}{\partial z}\left(K_u^n\frac{\partial\mathbf{u}^{n+1}}{\partial z}\right), \tag{10}$$

$$\frac{b^{n+1}-b^{n}}{\Delta t}=\frac{\partial}{\partial z}\left(K_b^n\frac{\partial b^{n+1}}{\partial z}\right), \tag{11}$$

$$\frac{(q^2)^{n+1}-(q^2)^{n}}{\Delta t}=2K_u^n(M^n)^2-2K_b^n(N^n)^2-\frac{2[(q^2)^n]^{5/2}}{16.6(q^2l)^n}+\frac{\partial}{\partial z}\left(K_q^n\frac{\partial(q^2)^{n+1}}{\partial z}\right), \tag{12}$$

$$\frac{(q^2l)^{n+1}-(q^2l)^{n}}{\Delta t}=1.8l^nK_u^n(M^n)^2-1.8l^nK_b^n(N^n)^2-\frac{W^n[(q^2)^n]^{3/2}}{16.6}+\frac{\partial}{\partial z}\left(K_q^n\frac{\partial(q^2)^{n+1}}{\partial z}\right). \tag{13}$$

All the non-linear terms are discretized explicitly in order to avoid solving a non-linear system. For the sake of clarity, we give in Appendix A the expression of Eqs. (12) and (13) where K_u^n, K_b^n, K_q^n, M^n, N^n and W^n have been expressed in terms of $\mathbf{u}^n$, b^n, $(q^2)^n$ and $(q^2l)^n$.

When discretizing Eqs. (3) and (4) in time, use is often made of the pseudo-implicit discretization of Patankar (1980) in order to avoid generating negative values of q^2 and q^2l (e.g., Deleersnijder and Luyten, 1994; Burchard and Beckers, 2004). This scheme however still requires to impose that l is bigger than a minimal value as it appears in the denominator of one of the terms in Eq. (3). However, in our implementation, better results were obtained by strongly imposing the following constraints:

$$q^2>q^2_{\min}\quad\text{and } q^2l>(q^2l)_{\min}$$

at the end of each time step rather than using a Patankar (1980) scheme. We therefore introduce $q^2_{\min}$ and $(q^2l)_{\min}$, the minimal values of q^2 and q^2l.

4. Numerical example: The Kato–Philips test case

The stress-driven penetration of a turbulent layer into a stratified fluid initially at rest is a classical test case to assess turbulence closure schemes in the context of marine modelling (e.g., Deleersnijder and Luyten, 1994; Burchard et al., 1998; Axell and Liungman, 2001; Burchard and Beckers, 2004). This experiment was first carried out in laboratory by Kato and Phillips (1969) with a non-rotating tank of fluid. The water column is considered sufficiently deep so that the only source of turbulence is the wind stress. Thus, the seabed has no influence on the flow and the wall proximity function, W, may be assumed to depend only on the distance to the surface.

The following initial and boundary conditions are used:

$$[\mathbf{u}, b]_{t=0} = [0, N_0^2 z],$$
$$[q^2, q^2 l]_{t=0} = [q^2_{\min}, (q^2 l)_{\min}],$$
$$\left[K_u \frac{\partial \mathbf{u}}{\partial z}, K_b \frac{\partial b}{\partial z}\right]_{z=0} = [\|\mathbf{u}_*\|\mathbf{u}_*, 0],$$
$$[q^2, q^2 l]_{z=0} = [6.5074\mathbf{u}_*^2, 0],$$

where N_0 is the initial Brunt-Väisälä frequency and $\mathbf{u}_*$ is the so-called surface friction velocity. The minimal values of q^2 and $q^2 l$ are set to $q^2_{\min} = 5 \times 10^{-7}\ \mathrm{m^2\ s^{-2}}$ and $(q^2 l)_{\min} = 10^{-5}\ \mathrm{m^3\ s^{-2}}$, respectively. At the bottom of the computational domain, homogeneous Neumann boundary conditions are enforced. As mentioned before, these conditions have no impact on the flow as the computational domain is supposed to be sufficiently deep. Following Deleersnijder and Luyten (1994), we transform this laboratory experiment to oceanic dimensions by setting $\|\mathbf{u}_*\| = 10^{-2}\ \mathrm{ms^{-1}}$ and $N_0 = 10^{-2}\ \mathrm{s^{-1}}$. The Coriolis factor is set to zero.

The convergence rate of the numerical scheme may be evaluated by computing the L_2-error on the numerical solution with respect to a high resolution solution computed on a mesh of 400 elements. The error on the velocity and buoyancy fields are defined as follows:

$$e_{\mathbf{u}} = \frac{\sqrt{\int_{-h}^{0} (u^r - u^h)^2 + (v^r - v^h)^2 \,\mathrm{d}z}}{\sqrt{\int_{-h}^{0} (u^r)^2 + (v^r)^2 \,\mathrm{d}z}}, \quad e_b = \frac{\sqrt{\int_{-h}^{0} (b^r - b^h)^2 \,\mathrm{d}z}}{\sqrt{\int_{-h}^{0} (b^r)^2 \,\mathrm{d}z}},$$

where the superscript r denotes the high-resolution reference solution. Both error measures are represented in Fig. 2 when using uniform meshes of 10, 20 and 40 elements and a time step of 60 s. As expected, quadratic convergence rates are observed.

For the case $f = 0$, Price (1979) suggested an analytical solution for the evolution of the mixed-layer depth D_m based on a constant bulk Richardson number

$$D_m(t) = 1.05\|\mathbf{u}_*\| N_0^{-1/2} t^{1/2}.$$

Fig. 3 shows the evolution of the mixed layer during 30 h of simulation. The computational domain is 40 m deep, the time step is set to 60 s, the mesh is uniform and composed of 40 elements. The analytical solution of Price (1979) is compared to numerical results obtained by defining the mixed layer depth as the depth at which the discrete TKE reaches values of 10^{-4} and $10^{-5}\ \mathrm{m^2\ s^{-2}}$. Decreasing the TKE threshold value increases the accuracy. However, for threshold values smaller than $10^{-5}\ \mathrm{m^2\ s^{-2}}$, the computed turbulent layer depth becomes noisy. Fig. 4 shows the profiles of buoyancy, velocity norm, TKE and mixing coefficients at the end of the simulation. These results are totally in line with those obtained by Deleersnijder and Luyten (1994) with a finite difference model.

5. Adaptive strategies

For applications like the deepening of the mixed layer under the influence of a wind stress, it is readily seen that better results could be obtained with non-uniform resolution. Indeed, the

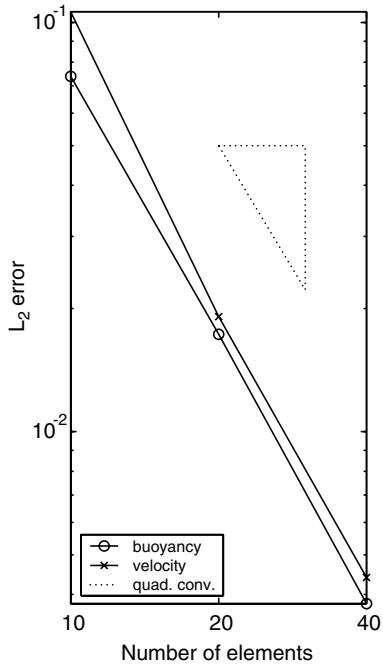

Fig. 2. L_2-error on the discrete buoyancy (○) and velocity (×) fields with different uniform meshes. The convergence rate is quadratic in each case.

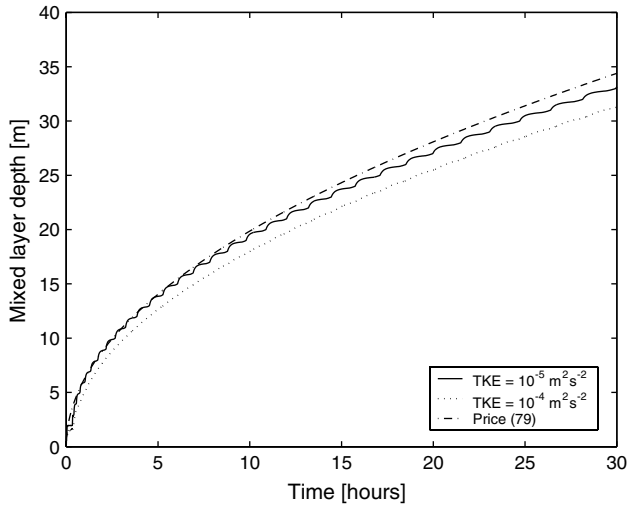

Fig. 3. Simulated mixed layer deepening compared to the algebraic solution of Price (1979). The numerical solutions are obtained by taking TKE threshold values of $10^{-4}\,m^2\,s^{-2}$ (···) and $10^{-5}\,m^2s^{-2}$ (—). The mesh is uniform and composed of 40 elements.

velocity and buoyancy solutions are quite smooth everywhere except near the surface and near the pycnocline (transition between the mixed and stratified layers). In these regions, the discrete

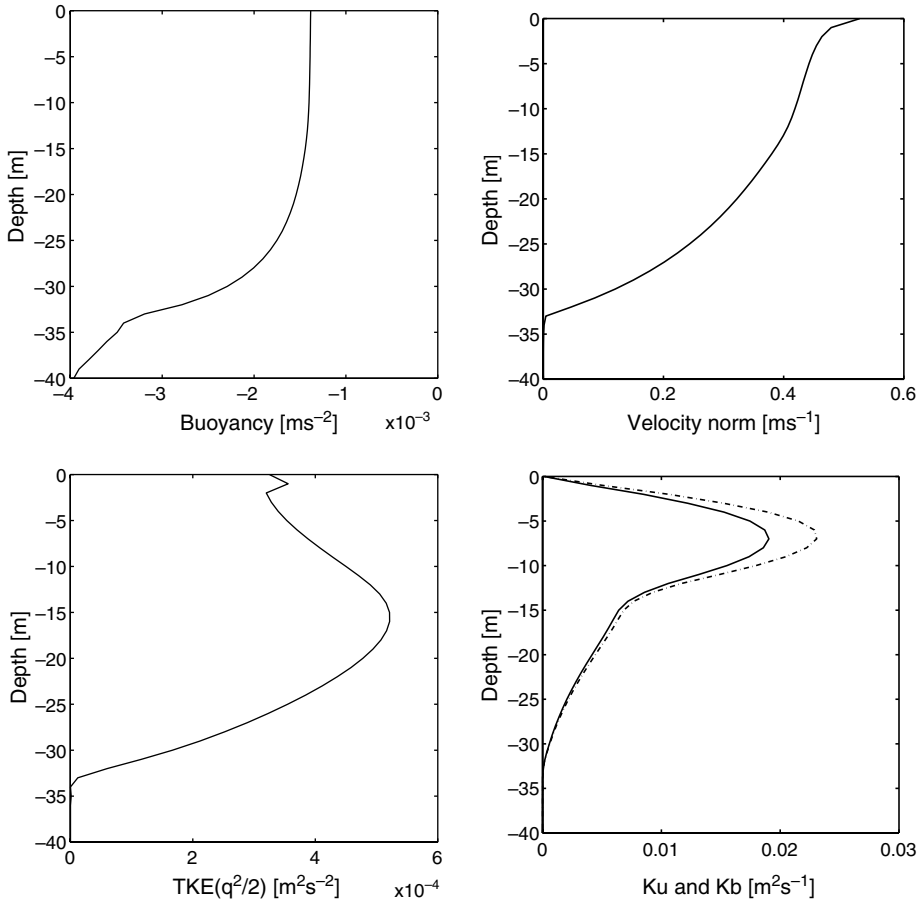

Fig. 4. Profiles of buoyancy, velocity norm, TKE and mixing coefficients K_u (—) and K_b (–·–) after 30 h for the simulation of the Kato–Phillips experiment. The mesh is uniform and composed of 40 elements.

solutions exhibit stronger gradients. However, since the depth of the mixed layer continuously increases, the resolution should also change accordingly. This can be achieved by using adaptive techniques. Such methods allow to change the resolution dynamically and fit very nicely within the finite element formalism.

The basic idea behind adaptivity is to compute, for a given discrete solution, an interpolation error. This can be done by using either an "a priori" or an "a posteriori" estimator of the discretization error. For instance, an "a priori" estimator may be based on the convergence order of the numerical method and an "a posteriori" estimator may be based on the knowledge of the physical phenomenon. Once the interpolation error is computed, a new mesh is built in order to evenly distribute the error on each element. In simple words, the resolution is increased where the error is large and decreased where the error is small. Our point here is not to review all the theory on which adaptive methods stand. Instead, we refer to the paper by Piggot et al. (2005) and the references therein for more information.

In this work, we present a simple example of adaptivity based on an heuristic "a posteriori" error measure. Following Burchard and Beckers (2004), we define the error on the numerical solution as:

$$e = e_b + e_u + e_d + e_k = c_b \frac{\max(N^2 - N_0^2, 0)}{\Delta b} + c_u \frac{M}{\Delta u} + c_d \frac{1}{d + d_0} + \frac{c_k}{d_{\max}}, \tag{14}$$

where Δb is a reference buoyancy difference, Δu is a reference velocity difference, d is the distance to the surface, d_0 is a variable that permits to tune the near-surface grid zooming and $d_{\max}$ is the depth of the domain. The coefficients c_b, c_u, c_d and c_k allow to set the relative importance of the four components of the error. The error is expressed in meters. With this expression for e, one may increase the resolution in region of strong shear, strong stratification and near the surface. The last component, e_k, is a background error that prevents too coarse resolution in regions with no shear, no stratification and far away from the surface. Again, we have to stress that this error estimator is very heuristic and only based on our knowledge of the physical phenomenon. Details on more rigorous "a posteriori" error estimates may be found in Strouboulis and Oden (1990), Cockburn and Gremaud (1996), Ainsworth and Oden (1997), Süli (1999) and Larson and Barth (2000).

Once an error measure has been derived, the nodes may be redistributed accordingly. As the accuracy of the finite element method depends both on the functional and geometrical discretizations, several strategies exist to uniformly distribute the interpolation error. One is to locally increase or decrease the degree of the finite element approximation. In 1D, this is quite straightforward as elements have at most one node in common. Reduction of the polynomial degree may be useful not only to reduce the accuracy of the solution, but also to eliminate spurious oscillations in the solution when non-smooth fields are present. Such an adaptive procedure is generally referred to as *p*-adaptivity. It is also possible to modify the numerical scheme accuracy by changing the geometrical discretization. This might be achieved by either moving the nodes location or by locally changing the mesh and its connectivity. The former method, refered to as *r*-adaptivity, does not change the topology and keeps the number of elements constant while the latter, refered to as *h*-adaptivity, allows to add and remove elements. When the number of elements remains the same, the movement of the grid may be taken into account by adding an advection term in the equations. The goal of this term is to counterbalance the movement of the mesh nodes and the advection velocity is simply the opposite of the mesh velocity. When the number of elements changes, mesh to mesh interpolation is required. It should be noted that it is possible to combine geometrical and functional modifications. in that case, the method is called *hp*-adaptive. Some authors also combine *h* and *r* methods to take advantage of both approaches (Piggot et al., 2005).

In this work, we have used only *r* and *h* adaptive methods. The *r*-adaptive procedure requires the introduction of a transport term in the discrete equations to compensate the motion of the grid. If the grid nodes are denoted $z_i(t)$ $(1 \leqslant i \leqslant N_E + 1)$, the vertical velocity at which a grid node moves is: $\tilde{w}_i(t) = \frac{\mathrm{d}z_i}{\mathrm{d}t}$. A continuous velocity field $\tilde{w}^h$ may then be built by linearly interpolating between vertical velocity nodal values. As an illustration of the modified equations, let us present the equation for the first component of the velocity:

$$\int_{-h}^{0} \frac{\partial u^h}{\partial t} \phi_i \,\mathrm{d}z + \int_{-h}^{0} \tilde{w}^h \frac{\partial u^h}{\partial z} \phi_i \,\mathrm{d}z - f \int_{-h}^{0} v^h \phi_i \,\mathrm{d}z = -\int_{-h}^{0} K_u \frac{\partial u^h}{\partial z} \frac{\partial \phi_i}{\partial z} \,\mathrm{d}z + (\tau^h_{0,x} - \tau^h_{-h,x}).$$

In matrix form, this yields:

$$\mathsf{M}_{ij}\left(\frac{\mathrm{d}u_j}{\mathrm{d}t} - fv_j\right) + \mathsf{A}_{ij}u_j = \mathsf{D}_{ij}u_j,$$

where $\mathsf{A}_{ij} = \int_{-h}^{0} \tilde{w}^h \phi_i \frac{\partial \phi_j}{\partial z}\,\mathrm{d}z$. This advection operator is centered in space and second order accurate if ϕ_i and ϕ_j are piecewise linear. This finite element scheme is conservative but does not guarantee monotonicity.

An example of *r*-adaptation is shown in Fig. 5. We start with a mesh $\{x_i, 1 \leqslant i \leqslant N_E + 1\}$ and a piecewise constant error field $e(x)$. We compute the error integral on each element: $E_i = \int_{x_i}^{x_{i+1}} e(x)\,\mathrm{d}x$ and on the whole domain: $E_{\mathrm{tot}} = \sum_{i=1}^{N_E} E_i$. A new mesh $\{x_i^*,\ 1 \leqslant i \leqslant N_E + 1\}$ is then built by imposing the following constraints:

$$E_i^* = \int_{x_i^*}^{x_{i+1}^*} e(x)\,\mathrm{d}x = \frac{E_{\mathrm{tot}}}{N_E},$$
$$x_0^* = x_0,$$
$$x_{N_E+1}^* = x_{N_E+1}.$$

This is achieved by successively moving the inner nodes of the initial mesh. When using a *h* method, one has to fix a priori an admissible error level per element: E^*. In that case, the new mesh is such that $E_i^* \leqslant E^*$. The number of elements may then change during the adaptation process.

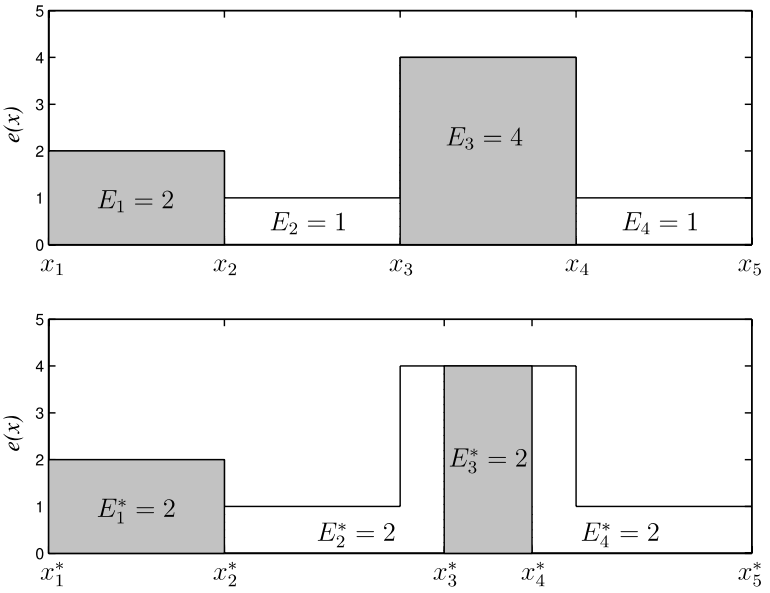

Fig. 5. Example of mesh adaptation. The initial mesh $\{x_i, 1 \leqslant i \leqslant 5\}$ is composed of 4 elements of unit length (top). By using an *r*-adaptive procedure, a new mesh $\{x_i^*,\ 1 \leqslant i \leqslant 5\}$ is obtained where the error ($e(x)$) is evenly distributed (bottom).

Fig. 6 shows the buoyancy field obtained with a *r*-adaptive scheme. The number of elements remains equal to 20 and the time step is set to 60 s. The following parameters have been used:

$$c_b = 1.2, \quad c_u = 0.0, \quad c_d = 0.3, \quad c_k = 0.75,$$
$$\Delta b = 0.002\ \mathrm{ms}^{-2}, \quad \Delta u = 0.2\ \mathrm{ms}^{-1}, \quad d_0 = 5.0\ \mathrm{m}, \quad d_{\max} = 40.0\ \mathrm{m}.$$

It can be seen that the mesh accurately follows the pycnocline. With an adaptive finite element scheme, the mixed layer deepens much more smoothly. This is illustrated in Fig. 7 where the mesh is only composed of 20 elements instead of 40 in Fig. 3. Fig. 8 shows the results obtained with a *h*-adaptive scheme. The error level per element is set to $E^* = 0.12$. The number of elements varies

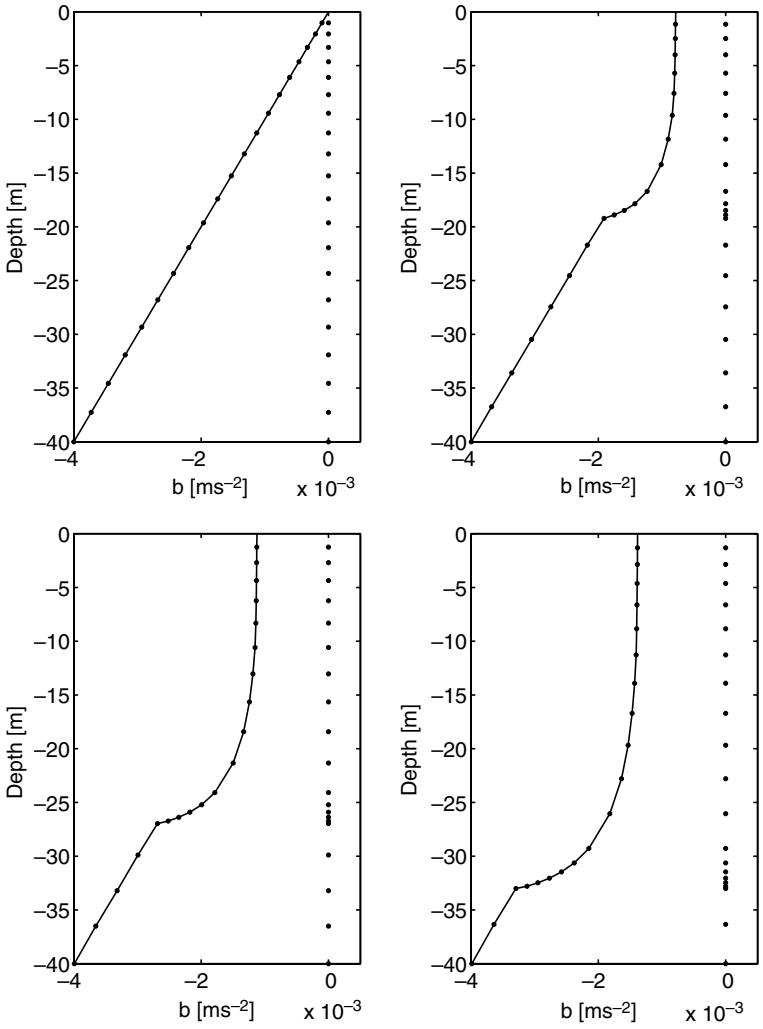

Fig. 6. Discrete buoyancy field after 0, 10, 20 and 30 h (from left to right) obtained with a *r*-adaptive scheme. The number of elements remains constant during the whole simulation. Mesh nodes are represented by "●".

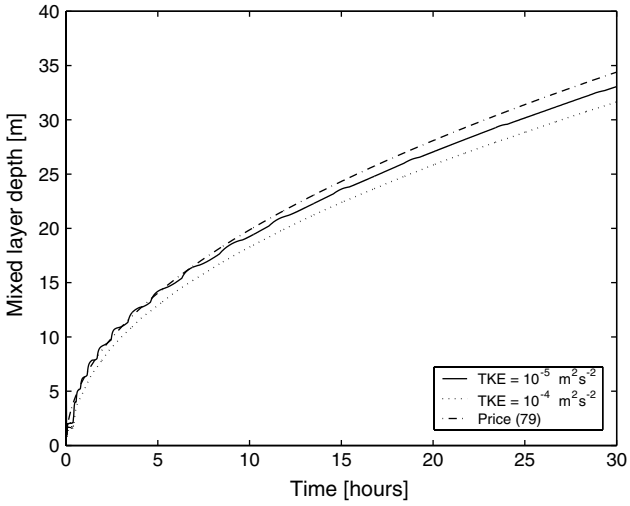

Fig. 7. Simulated mixed layer deepening compared to the algebraic solution of Price (1979). A *r*-adaptive scheme is used. The numerical solutions are obtained by taking TKE threshold values of 10^{-4} m^2 s^{-2} ($\cdots$) and 10^{-5} m^2 s^{-2} (—). The mesh is composed of 20 elements.

from 16 at the beginning to 23 by the end of the simulation and the average number of elements is 19.3. The time step is still equal to 60 s. To interpolate the discrete fields from the old mesh to the new one, we have used cubic Hermite interpolation scheme. This method preserves monotonicity and the shape of the data. It also has a slight smoothing effect that removes unwanted oscillations. The best accuracy could be obtained by using a least square projection as it minimizes the L_2-error between the initial and the interpolated fields. However, this method is not monotonous and may lead to negative buoyancy or velocity slope values.

As pointed out by Burchard and Beckers (2004) and Piggot et al. (2005), adaptive vertical meshes are expected to play a more important part in 3D ocean circulation models as they are able to achieve truly hybrid coordinates. Indeed, the free surface and bathymetry can be easily resolved while, in the mid-ocean, the mesh is free to follow isopycnals. Within our adaptive procedure, hybrid vertical coordinates may be obtained by defining an error estimator that depends on the distance to the surface, on the distance to the bottom and on the stratification. One of the main advantages of this adaptive strategy is that any "a priori" knowledge of the flow is needed to place vertical coordinates. As the mesh evolves with the internal structure of the flow, coordinate surfaces are always located in an optimal way. This prevents coordinate surfaces from vanishing when the flow becomes unstratified. It also prevents them from intersecting the sea surface or the sea bottom.

Finally, it should be noted that, in a 3D finite element model using prismatic elements, adjacent columns with a different number of elements may occur. These can result from the use of a *h*-adaptive scheme to move vertical coordinates or from bathymetry constraints. Indeed, changing the number of vertical levels may be necessary to represent sharp bathymetry variations, like those near the shelf-break (Deleersnijder and Beckers, 1992). In that case, the 3D mesh becomes non-conforming and a suitable numerical treatment should be performed.

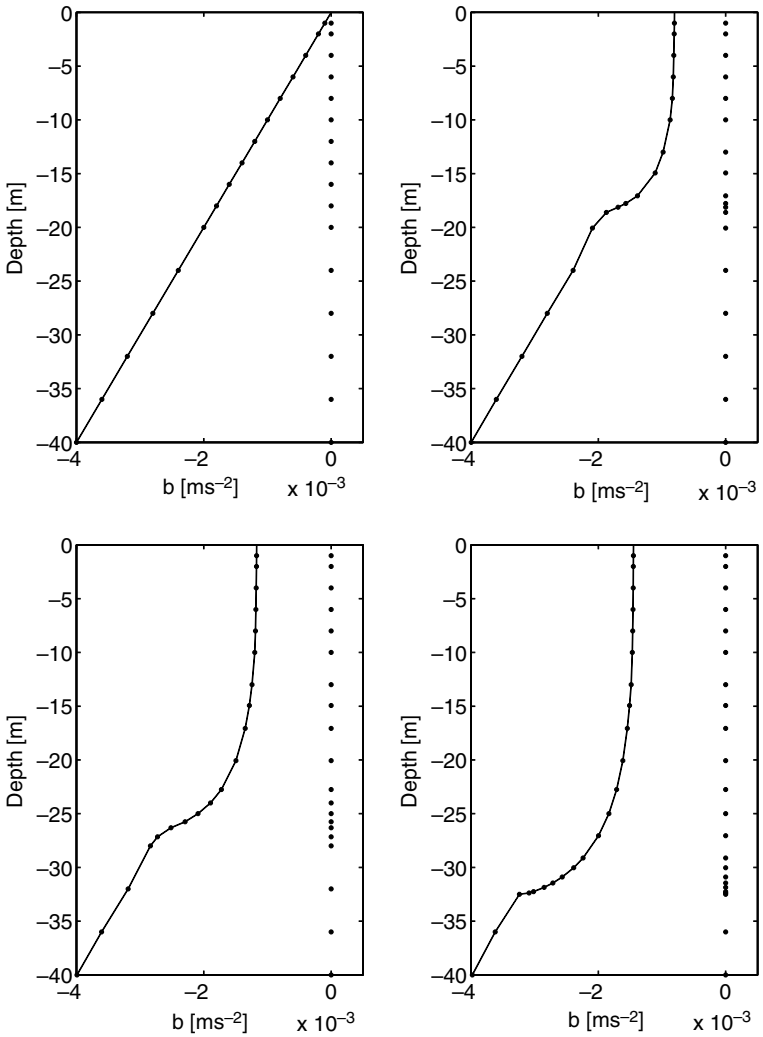

Fig. 8. Discrete buoyancy field after 0, 10, 20, 30 h (from left to right) obtained with a *h*-adaptive scheme. The meshes are composed of 16, 18, 20, 23 elements respectively. The mean number of elements over the whole simulation is 19.3. Mesh nodes are represented by "●".

6. Conclusions

We have built a simple finite element water column model using the Mellor and Yamada level 2.5 turbulence closure. All variables are approximated by piecewise linear polynomials and the eddy coefficients are piecewise constant. The model has been assessed by simulating the deepening of a stress driven turbulent layer into a stratified fluid. Results are comparable to those obtained with finite difference models.

Some adaptive strategies have also been proposed. These permit to dynamically change the mesh resolution. Hence, the physical phenomenon is always represented in an optimal way. In this

work, we have tested *r*- and *h*-adaptive schemes. The former keeps the number of elements constant and requires the addition of a transport term while the latter allows to change the number of elements during the simulation at the cost of mesh to mesh interpolations. Both methods have proved to be well suited to represent some internal structures of the flow, like the pycnocline position. Therefore, the finite element method with adaptive meshes seems to be a very promising method to represent horizontal but also vertical oceanic processes. Compared to more traditional numerical methods, it offers an increased flexibility and efficiency, which allows to resolve a broader range of length scales.

Acknowledgements

Emmanuel Hanert and Eric Deleersnijder are Postdoctoral Researcher and Research Associate, respectively, with the Belgian National Fund for Scientific Research (FNRS). The present study was carried out within the scope of the project "A second-generation model of the ocean system", which is funded by the *Communauté Française de Belgique*, as *Actions de Recherche Concertées*, under the contract ARC 04/09-316. This work is a contribution to the development of SLIM, the Second-generation Louvain-la-neuve Ice-ocean Model. We would like to thank Prof. Hans Burchard for providing detailed and insightful comments on our manuscript.

Appendix A. Expression of the model equations in terms of the primal variables

In this section, we present the expression of the model equations in terms of the primal variables $\mathbf{u}$, b, q^2 and $q^2 l$. This permits to highlight the non-linearity of the Mellor–Yamada level 2.5 turbulence closure. The equations for q^2 and $q^2 l$ may be written as:

$$\frac{(q^2)^{n+1}-(q^2)^n}{\Delta t}=2K_u^n\left\|\frac{\partial \mathbf{u}^n}{\partial z}\right\|^2-2K_b^n\frac{\partial b^n}{\partial z}-\frac{2[(q^2)^n]^{5/2}}{16.6(q^2 l)^n}+\frac{\partial}{\partial z}\left(K_q^n\frac{\partial(q^2)^{n+1}}{\partial z}\right), \tag{A.1}$$

$$\begin{aligned}\frac{(q^2 l)^{n+1}-(q^2 l)^n}{\Delta t}&=1.8\frac{(q^2 l)^n}{(q^2)^n}K_u^n\left\|\frac{\partial \mathbf{u}^n}{\partial z}\right\|^2-1.8\frac{(q^2 l)^n}{(q^2)^n}K_b^n\frac{\partial b^n}{\partial z}\\&\quad-\left(1+\frac{1.33[(q^2 l)^n]^2}{(\kappa z)^2[(q^2)^n]^2}\right)\frac{[(q^2)^n]^{3/2}}{16.6}+\frac{\partial}{\partial z}\left(K_q^n\frac{\partial(q^2)^{n+1}}{\partial z}\right),\end{aligned} \tag{A.2}$$

where

$$K_u^n=\frac{(q^2 l)^n}{\sqrt{(q^2)^n}}\frac{0.393+3.085\dfrac{[(q^2 l)^n]^2}{[(q^2)^n]^3}\dfrac{\partial b^n}{\partial z}}{1+40.083\dfrac{[(q^2 l)^n]^2}{[(q^2)^n]^3}\dfrac{\partial b^n}{\partial z}+212.469\dfrac{[(q^2 l)^n]^4}{[(q^2)^n]^6}\left(\dfrac{\partial b^n}{\partial z}\right)^2},$$

$$K_b^n = \frac{(q^2 l)^n}{\sqrt{(q^2)^n}} \frac{0.494}{1 + 34.676 \frac{[(q^2 l)^n]^2}{[(q^2)^n]^3} \frac{\partial b^n}{\partial z}},$$

$$K_q^n = 0.2 \frac{(q^2 l)^n}{\sqrt{(q^2)^n}}.$$

References

Ainsworth, M., Oden, J.T., 1997. A posteriori error estimation in finite element analysis. Computer Methods in Applied Mechanics and Engineering 142, 1–88.

Axell, L.B., Liungman, O., 2001. A one-equation turbulence model for geophysical applications: Comparison with data and the k–ε model. Environmental Fluid Mechanics 1, 71–106.

Blumberg, A.F., Mellor, G.L., 1987. A description of a coastal ocean circulation model. In: Heaps, N.S. (Ed.), Three Dimensional Ocean Models. American Geophysical Union Inc., Washington, DC, pp. 1–16.

Blumberg, A.F., Galperin, B., O'Connor, D.J., 1992. Modeling vertical structure of open-channel flows. Journal of Hydraulic Engineering 118 (H8), 1119–1134.

Burchard, H., 2001. Note on the $q^2 l$ equation by Mellor and Yamada (1982). Journal of Physical Oceanography 31, 1377–1387.

Burchard, H., 2002a. Applied turbulence modelling in marine waters. Lecture Notes in Earth Science, No. 100. Springer, Berlin.

Burchard, H., 2002b. Energy-conserving discretization of turbulent shear and buoyancy production. Ocean Modelling 4, 347–361.

Burchard, H., Beckers, J.-M., 2004. Non-uniform adaptive vertical grids in one-dimensional numerical ocean models. Ocean Modelling 6, 51–81.

Burchard, H., Bolding, K., 2001. Comparative analysis of four second-moment turbulence closure models for the oceanic mixed layer. Journal of Physical Oceanography 31, 1943–1968.

Burchard, H., Petersen, O., 1999. Models of turbulence in the marine environment—A comparative study of two-equation turbulence models. Journal of Marine Systems 21, 29–53.

Burchard, H., Petersen, O., Rippeth, T., 1998. Comparing the performances of the Mellor–Yamada and the k–ε two-equation turbulence models. Journal of Geophysical Research 103, 10543–10554.

Canuto, V.M., Howard, A., Cheng, Y., Dubovikov, M.S., 2001. Ocean turbulence. Part I: One point closure model. Momentum and heat vertical diffusivities. Journal of Physical Oceanography 31, 1413–1426.

Casulli, V., Walters, R.A., 2000. An unstructured grid, three-dimensional model based on the shallow water equations. International Journal for Numerical Methods in Fluids 32, 331–348.

Chen, C., Liu, H., Beardsley, R.C., 2003. An unstructured grid, finite-volume, three-dimensional, primitive equations ocean model: Applications to coastal ocean and estuaries. Journal of Atmospheric and Oceanic Technology 20, 159–186.

Ciarlet, P.G., 1978. The finite element method for elliptic problems. Studies in Mathematics and its Applications. North-Holland Publishing Company.

Cockburn, B., Gremaud, P.A., 1996. Error estimates for finite element methods for nonlinear conservation laws. SIAM Journal on Numerical Analysis 33, 522–554.

Cockburn, B., Karniadakis, G.E., Shu, C.W., 2000. Discontinuous Galerkin methods. Theory, computation and applications. Lecture Notes in Computational Science and Engineering. Springer, Berlin.

Danilov, S., Kivman, G., Schröter, J., 2004. A finite element ocean model: Principles and evaluation. Ocean Modelling 6, 125–150.

Davies, A.M., 1987. Spectral models in continental shelf sea oceanography. In: Heaps, N.S. (Ed.), Three-Dimensional Coastal Ocean Models, vol. 4. AGU, Washington DC, pp. 71–106.

Davies, A.M., Jones, J.E., 1991. On the numerical solution of the turbulence energy equations for wave and tidal flows. International Journal of Numerical Methods in Fluids 12, 17–41.

Deleersnijder, E., Beckers, J.-M., 1992. On the use of the σ-coordinate system in regions of large bathymetric variations. Journal of Marine Systems 3, 381–390.

Deleersnijder, E., Luyten, P., 1994. On the practical advantages of the quasi-equilibrium version of the Mellor and Yamada level 2.5 turbulence closure applied to marine modelling. Applied Mathematical Modelling 18, 281–287.

Ford, R., Pain, C.C., Piggot, M., Goddard, A., de Oliveira, C.R., Umpleby, A., 2004a. A non-hydrostatic finite element model for three-dimensional stratified oceanic flows, Part I: Model formulation. Monthly Weather Review 132, 2816–2831.

Ford, R., Pain, C.C., Piggot, M., Goddard, A., de Oliveira, C.R., Umpleby, A., 2004b. A non-hydrostatic finite element model for three-dimensional stratified oceanic flows, Part II: Model validation. Monthly Weather Review 132, 2832–2844.

Galperin, B., Kantha, L.H., Hassid, S., Rosati, S., 1988. A quasi-equilibrium turbulent energy model for geophysical flows. Journal of Atmospheric Sciences 45, 55–62.

Hanert, E., Le Roux, D.Y., Legat, V., Deleersnijder, E., 2005. An efficient Eulerian finite element method for the shallow water equations. Ocean Modelling 10, 115–136.

Iskandarani, M., Haidvogel, D.B., Boyd, J.B., 1995. A staggered spectral element model with application to the oceanic shallow water equations. International Journal for Numerical Methods in Fluids 20, 393–414.

Iskandarani, M., Haidvogel, D.B., Levin, J.C., 2003. A three-dimensional spectral element model for the solution of the hydrostatic primitive equations. Journal of Computational Physics 186, 397–425.

Johnson, C., 1990. Numerical Solution of Partial Differential Equations by the Finite Element Method. Cambridge University Press, Cambridge, MA.

Kantha, L.H., Clayson, C.A., 1994. An improved mixed layer model for geophysical applications. Journal of Geophysical Research 99, 25235–25266.

Kato, H., Phillips, O.M., 1969. On the penetration of a turbulent layer into stratified fluid. Journal of Fluid Mechanics 37, 643–655.

Larson, M., Barth, T., 2000. A posteriori error estimation for discontinuous Galerkin approximations of hyperbolic systems. In: Cockburn, B., Karniadakis, G., Shu, C.-W. (Eds.), Discontinuous Galerkin Methods. Theory, Computation and Applications. Springer, Berlin, pp. 363–368.

Le Roux, D.Y., Staniforth, A., Lin, C.A., 2000. A semi-implicit semi-Lagrangian finite-element shallow-water ocean model. Monthly Weather Review 128, 1384–1401.

Legrand, S., Legat, V., Deleersnijder, E., 2000. Delaunay mesh generation for an unstructured-grid ocean general circulation model. Ocean Modelling 2, 17–28.

Lynch, D.R., Ip, J.T.C., Naimie, C.E., Werner, F.E., 1996. Comprehensive coastal circulation model with application to the Gulf of Maine. Continental Shelf Research 16, 875–906.

Mellor, G.L., Yamada, T., 1974. A hierarchy of turbulence closure models for planetary boundary layers. Journal of the Atmospheric Sciences 31, 1791–1806.

Mellor, G.L., Yamada, T., 1982. Development of a turbulence closure model for geophysical fluids problems. Review of Geophysics and Space Physics 20, 851–875.

Patankar, S.V., 1980. Numerical Heat Transfer and Fluid Flow. Hemisphere, New York.

Piggot, M.D., Pain, C.C., Goreman, G.J., Power, P.W., Goddard, A.J.H., 2005. *h*, *r* and *hr* adaptivity with applications in numerical ocean modelling. Ocean Modelling 10, 95–113.

Price, J.F., 1979. On the scaling of stress-driven entrainment experiments. Journal of Fluid Mechanics 90, 509–529.

Rodi, W., 1987. Examples of calculation methods for flow and mixing in stratified fluids. Journal of Geophysical Research 92 (C5), 5305–5328.

Rosati, A., Miyakoda, K., 1988. A general circulation model for upper ocean circulation. Journal of Physical Oceanography 18, 1601–1626.

Strouboulis, T., Oden, J.T., 1990. A posteriori error estimation of finite element approximations in fluid mechanics. Computer Methods in Applied Mechanics and Engineering 78, 201–242.

Süli, E., 1999. A posteriori error analysis and adaptivity for finite element approximations of hyperbolic problems. In: An Introduction to Recent Developments in Theory and Numerics for Conservation Laws. In: Kroner, D.,

Ohlberger, Rhode, C. (Eds.), Lecture Notes in Computational Science and Engineering, vol. 5. Springer-Verlag, Berlin, pp. 123–194.

Timmermann, R., Beckmann, A., 2004. Parameterization of vertical mixing in the Weddell Sea. Ocean Modelling 6, 83–100.

Umlauf, L., Burchard, H., 2003. A generic length-scale equation for geophysical turbulence models. Journal of Marine Research 61, 235–265.

Umlauf, L., Burchard, H., Hutter, K., 2003. Extending the k–ω turbulence model towards oceanic applications. Ocean Modelling 5, 195–218.

Wilcox, D.C., 1988. Reassessment of the scale-determining equation for advanced turbulence models. AIAA Journal 26, 1299–1310.

Yamada, T., 1983. Simulations of nocturnal drainage flows by a q^2l turbulence closure model. Journal of the Atmospheric Sciences 40, 91–106.